

---

This is an electronic reprint of the original article.  
This reprint may differ from the original in pagination and typographic detail.

Chen, Yang; Anttu, Nicklas; Sivakumar, Sudhakar; Gompou, Eleni; Magnusson, Martin  
**Optical far-field extinction of a single GaAs nanowire towards in situ size control of aerotaxy nanowire growth**

*Published in:*  
Nanotechnology

*DOI:*  
[10.1088/1361-6528/ab5fe4](https://doi.org/10.1088/1361-6528/ab5fe4)

Published: 09/01/2020

*Document Version*  
Publisher's PDF, also known as Version of record

*Published under the following license:*  
CC BY

*Please cite the original version:*  
Chen, Y., Anttu, N., Sivakumar, S., Gompou, E., & Magnusson, M. (2020). Optical far-field extinction of a single GaAs nanowire towards in situ size control of aerotaxy nanowire growth. *Nanotechnology*, 31(13), Article 134001. <https://doi.org/10.1088/1361-6528/ab5fe4>

---

This material is protected by copyright and other intellectual property rights, and duplication or sale of all or part of any of the repository collections is not permitted, except that material may be duplicated by you for your research use or educational purposes in electronic or print form. You must obtain permission for any other use. Electronic or print copies may not be offered, whether for sale or otherwise to anyone who is not an authorised user.

PAPER • OPEN ACCESS

## Optical far-field extinction of a single GaAs nanowire towards *in situ* size control of aerotaxy nanowire growth

To cite this article: Yang Chen *et al* 2020 *Nanotechnology* **31** 134001

View the [article online](#) for updates and enhancements.



**IOP | ebooks™**

Bringing you innovative digital publishing with leading voices to create your essential collection of books in STEM research.

Start exploring the collection - download the first chapter of every title for free.

# Optical far-field extinction of a single GaAs nanowire towards *in situ* size control of aerotaxy nanowire growth

Yang Chen<sup>1</sup> , Nicklas Anttu<sup>2</sup> , Sudhakar Sivakumar<sup>1</sup> ,  
Eleni Gompou<sup>1</sup> and Martin H Magnusson<sup>1</sup>

<sup>1</sup> Solid State Physics, Lund University, Box 118, SE-22100 Lund, Sweden

<sup>2</sup> Department of Electronics and Nanoengineering, Aalto University, Aalto, Finland

E-mail: [yang.chen@ff.lth.se](mailto:yang.chen@ff.lth.se)

Received 18 June 2019, revised 13 September 2019

Accepted for publication 12 November 2019

Published 9 January 2020



CrossMark

## Abstract

A substrate-free approach of semiconductor nanowire growth has been achieved by the aerotaxy technique previously. In this work, we propose an *in situ* method to monitor the size of nanowires through non-destructive optical-extinction measurements. Our work aims to build a theoretical look-up database of extinction spectra for a single nanowire of varying dimensions. We describe the origin of possible peaks in the spectra, for example due to nanowire-length dependent Fabry–Perot resonances and nanowire-diameter dependent TM and TE mode resonances. Furthermore, we show that the Au catalyst on top of the nanowire can be ignored in the simulations when the volume of the nanowire is an order of magnitude larger than that of the Au catalyst and the diameter is small compared to the incident wavelength. For the calculation of the extinction spectra, we use the finite element method, the discrete dipole approximation and the Mie theory. To compare with experimental measurements of randomly oriented nanowires, we perform an averaging over nanowire orientation for the modeled results. However, in the experiments, nanowires are accumulating on the quartz window of the measurement setup, which leads to increasing uncertainty in the comparison with the experimental extinction spectra. This uncertainty can be eliminated by considering both a sparse and a dense collection of nanowires on the quartz window in the optical simulations. Finally, we create a database of extinction spectra for a GaAs nanowire of varying diameters and lengths. This database can be used to estimate the diameter and the length of the nanowires by comparing the position of a peak and the peak-to-shoulder difference in the extinction spectrum. Possible tapering of nanowires can be monitored through the appearance of an additional peak at a wavelength of 700–800 nm.

Supplementary material for this article is available [online](#)

Keywords: semiconductor nanowire, light scattering, aerotaxy growth

(Some figures may appear in colour only in the online journal)

## Introduction

Semiconductor nanowires are promising candidates for next-generation optoelectronic devices due to their strong light trapping ability and lower material consumption. Nanowires can be obtained for example by selective etching from planar structures [1] or by epitaxial growth on top of a substrate



Original content from this work may be used under the terms of the [Creative Commons Attribution 3.0 licence](#). Any further distribution of this work must maintain attribution to the author(s) and the title of the work, journal citation and DOI.

[2, 3]. Those nanowires can be further processed to devices like light-emitting diodes [4–6], solar cells [1, 2, 7–9] and photodetectors [10–13]. Recently, substrate-free growth of III-V semiconductor nanowires has been demonstrated with the aerotaxy technique, which holds promise for solar cell production due to its lower cost and higher growth rate [14, 15].

In aerotaxy, nano-sized Au particles are flown into a growth chamber together with organometallic gas precursors. Importantly, in aerotaxy, the nanowire growth occurs in the gas phase from the Au particles without the need of a growth substrate. The growth rate is up to  $1 \mu\text{m s}^{-1}$ , which is typically 20–1000 times higher than in traditional substrate-based processes [16, 17]. However, due to this high growth rate, it is challenging to control the size of the nanowires during growth.

To determine the size of the nanowires *in situ* during growth, we propose a non-destructive optical monitoring method: a beam of light is sent through an analysis chamber directly downstream the growth chamber where it interacts with the nanowires in the gas flow, and the transmitted spectrum is recorded, as shown in figure 1(a). By analyzing/comparing the recorded spectrum with results from electromagnetic modeling, we can extract the nanowire dimensions for real-time feedback to the ongoing growth, in order to optimize the size of subsequently fabricated nanowires.

To enable such characterization, we must be able to simulate the scattering of light from nanowires in the gas flow. In the aerotaxy growth, the nanowires are quite sparse with a typical density of  $10^6$  nanowires  $\text{cm}^{-3}$ . Thus, the average distance between neighboring nanowires is about  $100 \mu\text{m}$ , which is much larger than the incident wavelength of about  $0.5 \mu\text{m}$ . We assume that multiple scattering between nanowires can be neglected. Therefore, on the theoretical side, the problem reduces to the simulation of the optical response of a single nanowire and subsequent averaging for random nanowire orientation, to mimic the expected random orientation of each nanowire in the gas flow.

Here, we performed optical simulations to study how the optical response of a nanowire depends on the orientation, diameter, and length of the nanowire. We performed simulations with three methods to calculate the far field optical response of a single nanowire: (1) the finite element method (FEM) [18], (2) the discrete dipole approximation (DDA) [19–21] and (3) the Mie scattering theory [22, 23]. We discuss the benefits and drawbacks of each of these methods. After that, the simulation results are compared to measurements, and we give guidelines for further development of the measurement setup and conditions.

## Result and discussion

In the simulations, we solved the Maxwell equations for the light absorption and scattering. We used tabulated refractive index of GaAs and Au to describe the optical properties of the materials [24, 25].

As shown in figure 1(a), the nanowires are floating in the analysis chamber with randomly distributed orientations. A hemispherical Au particle on one tip of the nanowire is shown as a catalyst. An average over both polar angle  $\theta_{\text{NW}}$  and azimuth angle  $\varphi_{\text{NW}}$  should be done to calculate the transmission spectrum of the floating nanowires, together with an averaging over TE and TM polarization of the incident light. Note that this polarization average simulates the unpolarized light in the experiments. Importantly, the scattering and absorption cross sections do not depend on  $\varphi_{\text{NW}}$  after averaging over the incident polarization (see figure S1 in the supporting information, available online at [stacks.iop.org/NANO/31/134001/mmedia](https://stacks.iop.org/NANO/31/134001/mmedia)). Therefore, in the calculations, we model for fixed  $\varphi_{\text{NW}} = 0$  and average over just  $\theta_{\text{NW}}$  when considering a randomly oriented nanowire. However, due to the varying  $\varphi_{\text{NW}}$ , the probability to find a nanowire at  $\theta_{\text{NW}}$  is highest for  $\theta_{\text{NW}} = 90^\circ$  and smallest for  $\theta_{\text{NW}} = 0^\circ$ . The probability to find a randomly oriented nanowire with  $\theta_{\text{NW}}$  can be calculated (see figure S2 in supporting information), which we used in the averaging over  $\theta_{\text{NW}}$ . This modeling with one fixed  $\varphi_{\text{NW}}$  and varying  $\theta_{\text{NW}}$  can speed up the calculation by 1–2 orders of magnitude compared with a modeling where both  $\varphi_{\text{NW}}$  and  $\theta_{\text{NW}}$  are varied.

In this work, we define TE and TM polarized incident light such that the electric field of TE is along the  $x$ -direction as shown in figure 1(a) [26, 27]. The electric field of TM is along the  $y$ -direction. The scattering cross sections and absorption cross sections are defined as the ratio between scattered power (absorbed power) and incident light intensity. Thus those cross sections have the unit of area, and they denote the area from which the nanowire appears to scatter (absorb) the incident light. The extinction cross section is defined as the sum of the scattering and the absorption cross section.

For the optical response of the nanowire, the nanowire diameter, nanowire length, incident wavelength and the effect of the Au particle on top of the nanowire should be taken into consideration. We start with placing a nanowire along the  $y$ -direction with a diameter of 80 nm and consider wavelengths in the 300–850 nm range. In figures 1(b)–(d), we select three lengths for the nanowire without an Au particle on top: 100, 600 and 2000 nm, corresponding to much smaller, comparable and much longer than the incident wavelengths. At short nanowire length, results from FEM and DDA agree very well both for scattering cross section and absorption cross section as shown in figures 1(b) and (c). This is reasonable as FEM and DDA both solve the same full 3D nanowire light-scattering problem. In contrast, in Mie theory, the nanowire is assumed infinitely long and the cross-section is obtained as per unit length. To compare with FEM and DDA, we multiply the cross-section from Mie theory with the length of the nanowire. Simulation results from Mie theory show a clear deviation from FEM and DDA results at a short nanowire length in figure 1(b). A 100 nm long nanowire with a diameter of 80 nm differs strongly from the assumption of the infinite cylinder, and it leads to the significant difference compared with the 3D solution for the actual, finite-length nanowire in FEM and DDA. This deviation is reduced when the length of the nanowire is

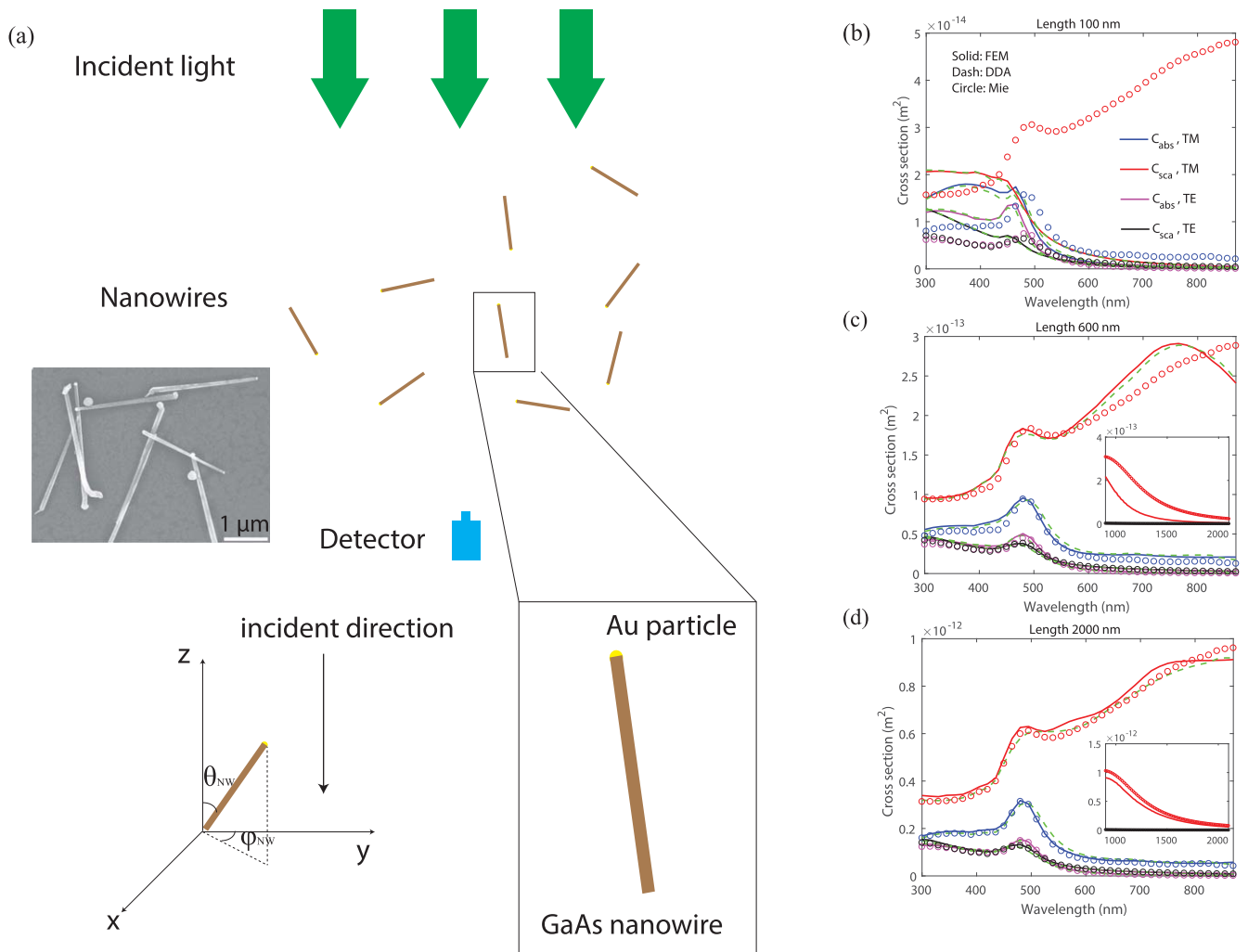


**Figure 1.** (a) Schematic drawing of designed *in situ* optical measurement. The direction of the nanowire is shown in the left bottom inset plot and defined by the angles  $\theta_{NW}$  and  $\varphi_{NW}$  with the light incident along the  $z$  direction. The SEM inset shows some GaAs nanowires grown by the aerotaxy technique. The typical lengths of such nanowires are at the level of micrometers and the diameter is several tens of nanometers. Those nanowires are deposited on the substrate after the growth and optical measurements. (b)–(d) Scattering and absorption cross sections calculated by the three methods (FEM, DDA, and Mie scattering theory) for a GaAs nanowire diameter of 80 nm and lengths of (b) 100 nm, (c) 600 nm, and (d) 2000 nm. The nanowire is placed along the  $y$ -direction ( $\theta_{NW} = 90^\circ$  and  $\varphi_{NW} = 0$ ). The color coding in (b) applies both to lines and circles in the plot, also for (c) and (d). Results from DDA are however shown with dashed green lines to distinguish them from the solid lines.

increased to 600 nm as shown in figure 1(c), especially at short wavelengths. In this situation, the diameter-to-length ratio is small, so that the finite-wire scattering has the potential to agree with Mie simulations. On the other hand, the incident wavelength can still be a limiting factor. In Mie theory, the wavelength is implicitly assumed much shorter than the length of the nanowire. Indeed, as seen from the FEM and DDA simulations, due to edge effects around the two tips of the nanowire, the scattering cross section shows a clear blue shift compared to results from Mie theory at long wavelengths, and the deviation is seen still at even longer wavelength as shown in the inset of figure 1(c). When we increase the length to 2 μm, the deviation at these longer wavelengths decreases (figure 1(d)). Similar results have been shown in a recent study of long silicon nanowires [28].

As a short summary, we can apply Mie theory only when the length of the nanowire is larger than or comparable to the

incident wavelength and when the length is much larger than the nanowire diameter. The use of Mie theory speeds up the computational time typically by 3 orders of magnitude compared to 3D modeling with DDA or FEM. For example, a single simulation run for a fixed orientation and wavelength took about 10–20 min with our FEM modeling in Comsol Multiphysics on a dual 16-core DELL Precision Tower 7910. Regardless of its time consumption, FEM has the merit of flexibility in changing the geometry and adding other materials. For instance, a study of the effect of the Au particle is easy to perform in FEM by adding a hemispherical Au particle on the tip of the nanowire. This is harder to do in the DDA implementation for which we use DDSCAT, and such a study of the effect of the Au particle is not possible in Mie theory. On the other hand, we found a smaller memory requirement in our typical modeling with DDSCAT than with FEM.

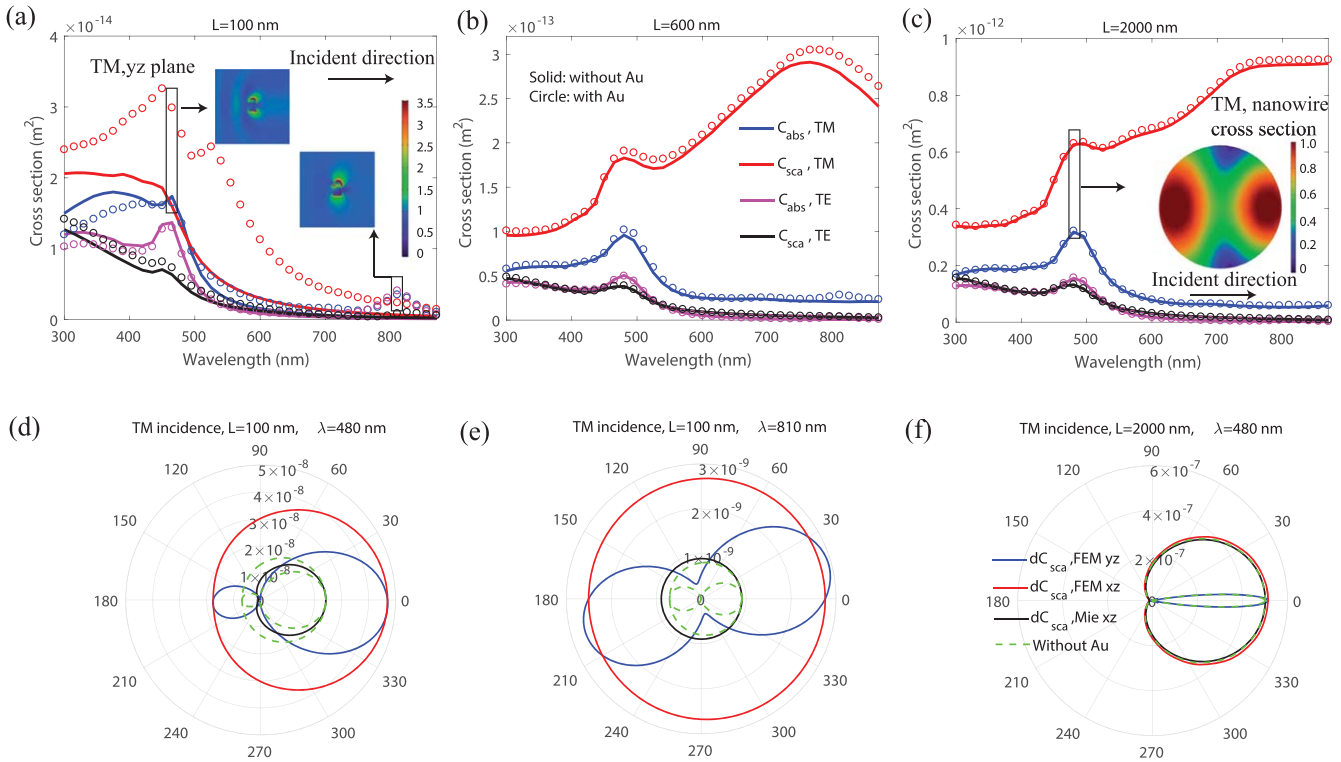


**Figure 2.** Scattering and absorption cross sections of a nanowire calculated by FEM, placed parallel to the  $y$ -direction (that is, with  $\theta_{NW} = 90^\circ$ ), with and without Au particle. (a) Nanowire length is 100 nm. (b) Nanowire length is 600 nm. (c) Nanowire length is 2000 nm. The insets of (a) and (c) show the electric field distribution  $|\mathbf{E}|$  (with a unit of  $\text{V m}^{-1}$  and the incident light having  $1 \text{ V m}^{-1}$ ) for a nanowire with Au particle and TM polarized incident light. The insets in (a) show  $|\mathbf{E}|$  at a wavelength of 480 nm and 810 nm respectively. The inset of (c) shows  $|\mathbf{E}|$  at a wavelength of 810 nm in the cross section of the nanowire (corresponding to the circle data point in the box marked in those figures). Figures (a)–(c) share the same legend as shown in (b). Figures (d)–(f) share the same legend as shown in (f) and show the directional scattering at absorption peaks in the direction  $\varphi_{sca}^r$ .  $\varphi_{sca}^r$  is the relative angle within that scattering plane where  $\varphi_{sca}^r = 0$  denotes the direction of incident light. Mie scattering results are normalized to the forward direction ( $\varphi_{sca}^r = 0$  in (d)–(f)) of finite wire  $dC_{sca}$ . (d) Nanowire length of 100 nm and incident wavelength of 480 nm. (e) Nanowire length of 100 nm and an incident wavelength of 810 nm. (f) Nanowire length of 2000 nm and an incident wavelength of 480 nm.

As an Au particle is not possible to include in Mie theory (since it requires a finite end of the nanowire), we employ FEM to study the effect of the Au particle in the light scattering process. In figure 2, we show cross sections of the nanowire with and without the Au particle on one tip of the nanowire. In this simulation, the shape of the Au particle is considered as a hemisphere. The diameter of the sphere is equal to the nanowire diameter.

In figure 2(a), for TM polarized incident light, a larger scattering cross is found for the nanowire with the Au particle. At a wavelength of 480 nm, the scattering cross section is about 50% larger than for the nanowire without an Au particle. The  $|\mathbf{E}|$  in the corresponding small inset in figure 2(a) shows a clear fringe pattern due to strong reverse scattering from the nanowire, which agrees with this scattering enhancement. In a short nanowire whose length is comparable to the diameter, this peak can be explained by the Mie mode resonance of a spherically shaped scatterer [29, 30]. With increasing nanowire length, this sphere-like mode gradually changes to the mode of an infinitely long nanowire [30, 31].

Note that in a nanowire array solar cell, normally incident light can excite guided HE modes at the top of the vertical nanowires, giving rise to absorption peaks [31, 32]. In

contrast, instead of guided modes, leaky TM or TE modes can give rise to peaks in the spectra of infinitely long nanowire [33–36]. Importantly, the Mie theory assumes an infinitely long nanowire, and hence, a peak seen in results from Mie theory cannot originate from guided HE modes.

As seen from figures 2(b) and (c), with increasing nanowire length, the cross sections for a nanowire with and without Au particle agree better. Thus, for longer nanowires, the nanowire dominates the scattering, and we assign the peak at around 480 nm in wavelength to the  $TE_{01}$  and the  $TM_{11}$  mode, for TE and TM polarized incident light, respectively. The inset in figure 2(c) is shown to illustrate the  $|\mathbf{E}|$  distribution for TM polarized incident light. The field distribution confirms the excitation of the  $TM_{11}$  mode [33]. From our results, it appears that we can ignore the Au particle when the semiconductor volume is an order of magnitude larger than that of the Au particle, as long as the diameter of the nanowire is much smaller than the wavelength of light. A recent study of a silicon nanowire showed a similar effect in the presence of a small Ag particle [37].

Besides this peak due to the  $TE_{01}/TM_{11}$  mode, two extra peaks occur for short nanowires when the Au particle is present. A scattering peak at around 525 nm is shown in

figure 2(a) and it approximately agrees with previously reported calculations of an Au sphere with a diameter of 80 nm which has a scattering peak at around 560 nm [34, 38], with a blue shift due to the presence of the semiconductor nanowire. In addition, a small scattering and absorption peak at around 810 nm occurs due to the presence of the Au particle. The large contrast in the dielectric constant between Au and air leads to a strong field enhancement around the nanoparticle, which leads to the enhancement of light scattering at long wavelengths. A near field plot is shown in the right inset of figure 2(a) and illustrates the strong localized field around the Au particle.

To give an insight into the light scattering, we calculate the differential scattering cross section. In three-dimensional scattering simulations, this differential cross section is calculated as:

$$dC_{3D} = \frac{dW}{I_0} = \frac{P}{I_0} dS = \frac{P}{I_0} 4\pi r^2 \frac{d\Omega}{4\pi} = \frac{P}{I_0} r^2 d\Omega, \quad (1)$$

where  $I_0$  is the incident intensity and  $P$  is the far field power flow. For a given direction in the far field, the scattered light can be approximated by a plane wave and the power flow can be calculated by  $P = \frac{cn\epsilon_0}{2} |E_{far}|^2$  (where  $n = 1$  is the refractive index used for the surrounding of the nanowire and  $E_{far}$  is the scattering far field).

On the other hand, due to the cylindrical symmetry of Mie scattering, the differential scattering cross section is calculated in a plane perpendicular to the nanowire axis and averaged over nanowire length [22]. According to the definition, the differential cross section in Mie scattering is:

$$dC_{Mie} = \frac{dC_{2D}}{L} = \frac{P}{I_0} 2\pi r \frac{d\varphi}{2\pi} = \frac{P}{I_0} r d\varphi, \quad (2)$$

where  $L$  is the length of the nanowire,  $dC_{2D}$  is the corresponding value comparing to  $dC_{3D}$ . As the absolute value of scattering intensity has been compared, we show  $dC_{sca} = \frac{dC_{3D}}{L}$  for FEM in figures 2(d)–(f) to illustrate the angular distribution of scattered light. In these figures, the Mie scattering results are normalized to the 3D finite wire simulation by forcing the forward direction to the same intensity and scaling the other directions with the same constant.

Firstly, in figure 2(d), we plot  $dC_{sca}$  corresponding to the parameters of the left inset in figure 2(a). Differential scattering cross sections are plotted in both the  $y$ - $z$  and  $x$ - $z$  planes for three-dimensional scattering with and without Au particle. The nanowire with an Au particle has a larger differential cross section than that of the nanowire without Au. Meanwhile, the distribution of scattered light keeps a similar shape in both the  $y$ - $z$  and  $x$ - $z$  plane. However, Mie theory, which can show scattering only in the  $x$ - $y$  plane for the  $y$ -oriented nanowires, shows a very different distribution with tiny backward reflection. This difference originates from the short length of the nanowire for which Mie theory cannot be reliably applied as discussed before.

Secondly, in figure 2(e), we plot  $dC_{sca}$  corresponding to parameters of the large inset in figure 2(a) to show a strong scattering enhancement at this wavelength. A clear non-symmetric distributed scattering pattern is shown in the  $y$ - $z$

plane. Comparing with the dashed green line, which is the scattering pattern of a nanowire without an Au particle, the distribution rotates anti-clockwise by about  $15^\circ$ . Thus, the strong scattering from the Au particle breaks the symmetry in scattering around the forward direction. Besides this change of the shape, the absolute value of the scattering cross section is also enhanced due to the presence of the Au particle.

Thirdly, in figure 2(f), we plot  $dC_{sca}$  corresponding to the parameters used for the inset in figure 2(c). We can see a very good angle-dependent agreement for the nanowire with and without Au particle. In addition to that, Mie theory also shows the same angle-dependent distribution as in three-dimensional results. It confirms the possibility of using Mie theory for long nanowires to approximate a nanowire with an Au particle at perpendicular incidence.

As a short summary, the Au particle plays an important role when the nanowire is short. We can ignore the effect of the Au particle when the following two conditions are fulfilled: (1) the volume of the nanowire is at least an order of magnitude larger than the volume of the Au particle, (2) and the diameter of the nanowire is much smaller than the wavelength.

In the calculations needed for extracting nanowire dimensions, we need to average over the different orientations of a nanowire and consider nanowires with different lengths and diameters. Besides the wavelength-dependent study, we also further study the diameter, length and orientation dependence of nanowires as shown in figure 3 for the specific case of illumination with a green laser of 532 nm in wavelength.

In figure 3(a), the absorption and scattering cross sections are shown for both TM and TE incidence as a function of nanowire diameter. TM incidence dominates the extinction cross sections due to its strong scattering cross section. With increasing diameter, we observe a list of peaks in the absorption cross section, which corresponds to the TM and TE mode of the infinite cylinder [33, 34]. At small diameters, the Au particle plays only a minor role because of its small volume compared to that of the semiconductor nanowire. With increasing diameter, the size of the Au particle becomes comparable to the incident wavelength. Such a large Au particle does not change the angular distribution of scattering as shown in figure 3(d), but it changes the absolute value of the scattering. We assign this change to the appearance of additional diffraction effects when the size of the Au particle is comparable to the incident wavelength, regardless of the large volume of the semiconductor nanowire.

In figure 3(b), the effect of the nanowire orientation is studied by changing the polar angle for a nanowire of 80 nm in diameter and 2000 nm in length. As shown in the plots, for this nanowire, for any  $\theta_{NW}$ , the Au particle shows a negligible effect in both absorption and scattering cross sections.

Interestingly, Mie theory shows very large discrepancies at a small polar angle and the cross-sections approach zero at  $\theta_{NW} = 0$ . This behavior is due to characteristics of the Hankel functions used in the Mie theory. Except for this limitation of the theory, the discrepancies between Mie theory and full 3D

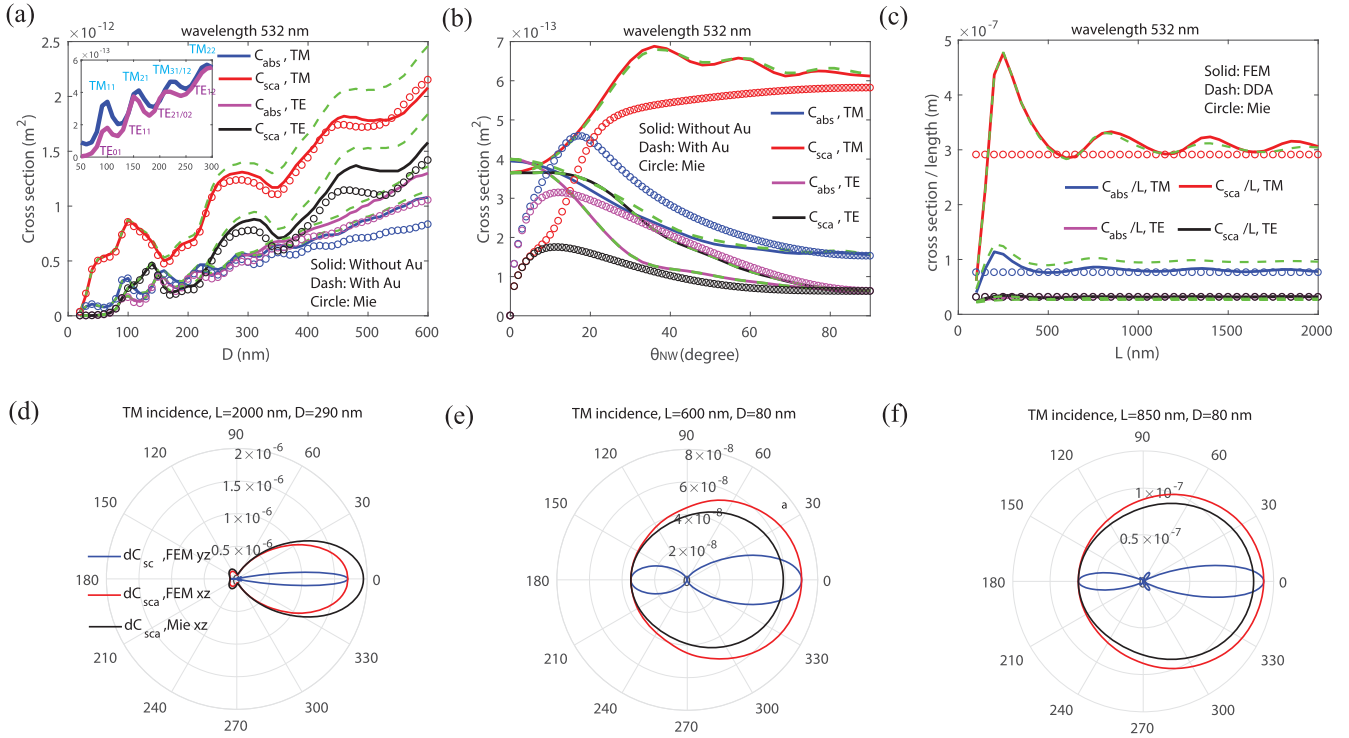


**Figure 3.** Scattering cross sections as a function of (a)  $D$ , the diameter of the nanowire, (b) polar angle  $\theta_{NW}$ , and (c)  $L$ , length of the nanowire. In (a) and (c), the polar angle is  $\theta_{NW} = 90^\circ$ . The diameter and length are 80 and 2000 nm if not specified. The inset of (a) shows the modes which are expected to give rise to the corresponding absorption peaks. The third peak that lays in between 200 and 250 nm in diameter is excited by two modes that are close to each other. (d)  $dC_{sca}$  polar plot for a diameter of 290 nm as a function of  $\theta_{sca}$ . (e)  $dC_{sca}$  polar plot for a length of 600 nm. (f)  $dC_{sca}$  polar plot for a length of 850 nm. Figures (e), (f) share the same legend as shown in (d). The Mie scattering results are normalized to  $dC_{sca}$  of a finite wire in the backward direction ( $\theta_{sca} = 180^\circ$  in (d)–(f)).

modeling may originate from the scattering at the tip of the nanowire. In our case, this effect is small at close to perpendicular incidence, that is, for  $\theta_{NW} \approx 90^\circ$ , but becomes larger at small polar angles. For this wavelength of 532 nm, we find a peak in the absorption and scattering cross-sections at  $\theta_{NW} \approx 10^\circ$ – $20^\circ$ , which qualitatively agrees with figure 6 in [30].

In figure 3(c), we compare the cross sections per unit length of nanowire as a function of nanowire length with the three methods. In our modeling, DDA gives a good agreement with FEM when calculating the scattering cross section, but it shows some noticeable discrepancy when calculating the absorption cross section. In our application, the extinction cross section is the final target and the absorption cross section is much smaller than the scattering cross section. Hence, DDA can be applied for our analysis. On the other hand, in contrast to the fluctuating values for the cross-section in the full 3D modeling, Mie theory gives length independent values for the cross-sections, and hence a fluctuating error with changing nanowire length. The separation in nanowire length of each neighboring peak in the full 3D modeling is about 500 nm, with valley to the peak distance of 250 nm on average. We assign this fluctuation to the Fabry–Perot resonance of light scattered between the tips of the nanowire. When the length increases, the transmission at top and bottom cross sections fluctuates, and it leads to the enhancement and suppression of scattered light intensities. To give further insight, we show two polar plots for the nanowire length of

600 nm (figure 2(e)) and 850 nm (figure 2(f)) corresponding to the valley and peak of the scattering cross section. At the length of 850 nm, both forward scattering and backward scattering are much stronger than for the length of 600 nm. The tiny branches around  $60^\circ$  and  $300^\circ$  scattering angles indicate the enhancement of transmission at the tips of the nanowire. But due to the diffraction effect at the nanoscale and the small surface size of the nanowire, this transmission enhancement mainly occurs in the forward and backward directions rather than in the perpendicular direction.

We assume that the nanowires have in the experiments an equal probability to point in any direction (the distribution, as a function of  $\theta_{NW}$  after integration over  $\varphi_{NW}$ , is shown in supporting information figure S2). In figure 4(b), we show an example plot of  $\theta_{NW}$  and  $\varphi_{NW}$  averaged extinction cross section of a two micrometer long nanowire, which is a typical length of aerotaxy GaAs nanowires. For this length of the nanowire, we can ignore the effect of the Au particle due to the large volume of nanowire as discussed above and shown in figure 2. A peak in the extinction spectra is found at around 500 nm in wavelength with a shoulder in the longer wavelength region. A clear blue shifting can be found for this extinction peak with decreasing nanowire diameter due to the mode shifting [31, 33, 34, 39]. In addition to the mode shifting, as the diameter decreases to below 60 nm, the extinction peak gradually vanishes, and a shoulder like structure occurs around a similar wavelength. This can be explained by the vanishing

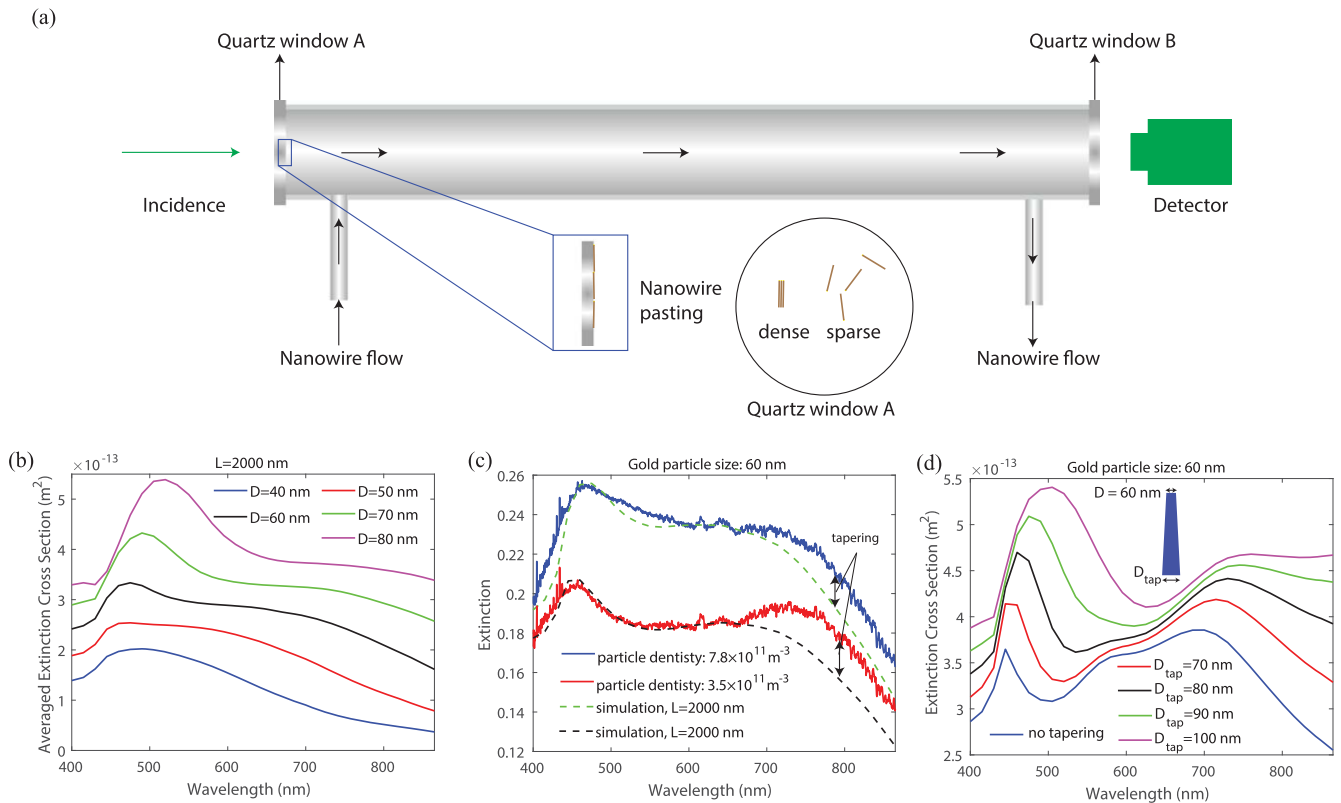


**Figure 4.** (a) Schematic drawing of the measurement setup. (b) Extinction cross sections average over nanowire orientation, that is, over  $\theta_{NW}$  and  $\varphi_{NW}$ . (c) Measured transmission spectra and numerical fitting. (d) Calculated tapered nanowire extinction spectra at perpendicular incidence ( $\theta_{NW} = 90^\circ$ ). The small tip of the nanowire has a diameter of 60 nm which is the same as the Au particle size. The large tip ranges from 70 to 100 nm in size as indicated by  $D_{tap}$  in the figure caption.

of the mode due to a cut off frequency, into which the mode shifts with decreasing diameter of the nanowire [40].

A database of GaAs nanowire spectra was built up with a diameter step of 5 nm and length step of 25 nm (an example plot of 3 micrometer long nanowires is shown as figure S3 in supporting information). This database can be used for extracting the nanowire dimensions by comparing with measured spectra. More precisely, the diameter of the nanowire can be extracted by the peak position of the transmission spectrum if the diameter is larger than 60 nm. As shown in figure 4(b), the shoulder-to-peak difference increases monotonously with increasing length. Ideally, we can extract the nanowire length from this increase in the measured spectra.

In the actual measurement, further technical issues with the setup arise. These issues affect the accuracy of this dimension extraction especially for the length of the nanowires. We measured and compared the results with the simulation in figure 4(c). In this comparison, we fitted the peak position of the measured spectra to the simulated spectra. A diameter of 60 nm is extracted and used in the plots. This diameter agrees with the measurement if tapering is not considered. (See table S1 in supporting information.) Regarding the nanowire length, ideally we can extract it from the absolute height of the peak and shoulder. However, as mentioned above, the pasting of nanowires on the window may change the absolute values in the spectra. Here we use the length extracted from SEM images. We measured a length

of  $2.3 \mu\text{m} \pm 0.3 \mu\text{m}$  from 132 nanowires on an area of  $0.271 \text{ cm}^2$ . In the numerical fitting, we take the value of  $2 \mu\text{m}$  as the nanowire length.

The schematic drawing of the measurement setup can be found in figure 4(a). The aerotaxy nanowires are injected from the growth chamber and they flow through a 60 cm long metal tube. The tube is connected optically with the incident light and the detector through two quartz glass windows. For the transmission spectrum, we average over 6000 measurements with an integration time of  $400 \mu\text{s}$  for each measurement. After this average, to normalize the data, we divided the measured intensity with nanowires by the measured intensity with only Au particles in the tube. Such transmission spectra are plotted as solid lines in figure 4(c). In addition, we consider the contribution of the faceted particles. Those faceted particles are formed in the growth as not all the material enters the Au catalyst. Those particles are seen in the inset of the SEM image in figure 1(a) as the round white particles attached to the nanowire. The composition of these particles can be Ga, As, GaAs or a mixture of semiconductor and metals. As the size is unknown as well, we simply assume that they contribute a constant, wavelength-independent background to the extinction of light. This background level is used as an unknown parameter in the fitting. All the parameters are listed in table S2 in the supporting information.

In figure 4(c), other optical losses are also considered in the simulation results. Due to the injection of nanowires as shown in figure 4(a), the nanowire can attach onto the glass window which is next to the injection channel. As time passes, more and more nanowires are attached to the window and the extinction of those nanowires should be included in the fitting. These attached nanowires can be classified into two types: (1). A sparse collection of nanowires which can be approximated as floating nanowires with their long axis perpendicular to the incidence direction. (2). A dense collection of nanowires together with faceted particles which can be approximated as a planar GaAs film with the thickness given by the nanowire diameter. The dense nanowires contribute mainly to the blue region of the extinction spectrum. (see figure S4 in support information). The sparse nanowires contribute on the other hand mostly to extinction at a longer wavelength. The parameters used in these modifications are also listed in table S2 of the supporting information. As those modification parameters are not known, we fitted the parameters to the shape and shoulder-to-peak height of the measurements. Such modification can fit the peak height and spectrum shape from 400 to 700 nm.

In addition to the agreement, we still found a deviation at long wavelengths. Such deviation cannot be fitted by changing the amount of attached nanowire on the window (ratio of perpendicular nanowires in the whole scattering process). We instead assign this deviation to the shape of the nanowire. That is to say, in the modeling, the nanowire is modeled as a homogeneous cylinder with a hemispherical Au particle on one tip as a catalyst. But in the aerotaxy growth, the nanowire may have a larger diameter at the end far from the catalyst [14] even with the recent improvements in the growth [16]. Such inhomogeneous diameter can lead to a higher absorption at longer wavelength [31, 32, 41]. To illustrate this effect, we calculate the extinction spectra of tapered nanowires and show them in figure 4(d). A clear extinction peak is shown at a wavelength around 700–800 nm and a red shifting of this peak is found as a function of increasing diameter. Such a red-shifting extinction peak of tapered nanowires can lead to enhancement of the extinction at long wavelengths, which could explain the difference between modeling and measurements in figure 4(c). Further optical simulation of the tapered nanowires should give better fitting to the experiments. However, usually, a tapered nanowire is not good for device fabrication. From the fabrication side, such tapering leads often to an increasing number of defects and increasing difficulty in device processing [41]. Thus, further experimental efforts should be carried out to optimize the shape of the nanowires and to limit the collection of nanowires to the measurement windows during growth.

## Conclusion

By applying Mie theory, FEM and DDA, we studied the optical extinction spectra of a single floating nanowire in the analysis chamber. The results from the FEM and the DDA agreed very well. The computationally fast Mie theory could

be applied only when (1) the length of the nanowires was larger than or comparable to the incident wavelength, (2) the length of the nanowires was much larger than the nanowire diameter, and (3) the angle between the incident light and the nanowire axis was larger than  $70^\circ$ . The Au catalyst could be ignored when the amount of semiconductor material in the nanowire was an order of magnitude larger than the amount of Au and the diameter was small compared to the incident wavelength. The effect of varying diameter, length and orientation of the nanowire was studied, and TM/TE mode resonances were found. With an increasing length, a clear Fabry–Perot resonance was found when analyzing the extinction cross section normalized to the length of the nanowire. By averaging the extinction over nanowire orientation, we compared simulation results with experimental measurements. We found an interesting background/noise, which is caused by nanowires accumulating on the quartz window in the measurement setup. After correcting for this background/noise in the optical simulations, we found a good agreement at the wavelength region of 400–700 nm, but still a deviation from 700 to 850 nm remained. We assigned this deviation to the tapering of the nanowires. As an outcome, we created a database of GaAs nanowire extinction spectra with a homogenous diameter for analyzing nanowire dimensions *in situ* during growth.

## Acknowledgments

This work was performed in NanoLund at Lund University and with financial support from the Swedish Research Council (VR) and from the Knut and Alice Wallenberg Foundation (KAW).

## ORCID iDs

Yang Chen  <https://orcid.org/0000-0002-8964-0084>  
 Nicklas Anttu  <https://orcid.org/0000-0002-7626-5107>  
 Sudhakar Sivakumar  <https://orcid.org/0000-0002-0205-9036>

## References

- [1] van Dam D *et al* 2016 High-efficiency nanowire solar cells with omnidirectionally enhanced absorption due to self-aligned indium–tin–oxide mie scatterers *ACS nano* **10** 11414
- [2] Wallentin J *et al* 2013 InP nanowire array solar cells achieving 13.8% efficiency by exceeding the ray optics limit *Science* **339** 1057–60
- [3] Wu Z *et al* 2002 Growth of Au-catalyzed ordered GaAs nanowire arrays by molecular-beam epitaxy *Appl. Phys. Lett.* **81** 5177–9
- [4] Minot E D *et al* 2007 Single quantum dot nanowire LEDs *Nano Lett.* **7** 367
- [5] Yan R *et al* 2009 Nanowire photonics *Nat. Photon.* **3** 569
- [6] Pan C F *et al* 2013 High-resolution electroluminescent imaging of pressure distribution using a piezoelectric nanowire LED array *Nat. Photon.* **7** 752

- [7] Åberg I *et al* 2015 A GaAs nanowire array solar cell with 15.3% efficiency at 1 sun *IEEE J. Photovolt.* **6** 185
- [8] Otnes G *et al* 2018 Understanding InP nanowire array solar cell performance by nanoprobe-enabled single nanowire measurements *Nano Lett.* **18** 3038–46
- [9] Yao M *et al* 2015 Tandem solar cells using GaAs nanowires on Si: design, fabrication, and observation of voltage addition *Nano Lett.* **15** 7217
- [10] Ren D *et al* 2019 Room-temperature midwavelength infrared InAsSb nanowire photodetector arrays with Al<sub>2</sub>O<sub>3</sub> passivation *Nano Lett.* **19** 2793
- [11] Svensson J *et al* 2013 Diameter-dependent photocurrent in InAsSb nanowire infrared photodetectors *Nano Lett.* **13** 1380
- [12] Svensson J *et al* 2017 Increased absorption in InAsSb nanowire clusters through coupled optical modes *Appl. Phys. Lett.* **110** 081104
- [13] Lee W-J *et al* 2015 High quantum efficiency nanopillar photodiodes overcoming the diffraction limit of light *Nano Lett.* **16** 199–204
- [14] Heurlin M *et al* 2012 Continuous gas-phase synthesis of nanowires with tunable properties *Nature* **492** 90
- [15] Magnusson M H *et al* 2014 Semiconductor nanostructures enabled by aerosol technology *Frontiers Phys.* **9** 398
- [16] Barrigón E *et al* 2017 GaAs nanowire pn-junctions produced by low-cost and high-throughput aerotaxy *Nano Lett.* **18** 1088
- [17] Metaferia W *et al* 2016 GaAsP nanowires grown by aerotaxy *Nano Lett.* **16** 5701
- [18] Comsol A B 2017 *Wave Optics Module User's Guide, COMSOL Multiphysics® v. 5.3a (Stockholm, Sweden)* pp 38–46
- [19] Draine B T and Flatau P J 2008 Discrete-dipole approximation for periodic targets: theory and tests *J. Opt. Soc. Am. A* **25** 2693
- [20] Draine B T and Flatau P J 1994 Discrete-dipole approximation for scattering calculations *J. Opt. Soc. Am. A* **11** 1491
- [21] Flatau P J and Draine B T 2012 Fast near field calculations in the discrete dipole approximation for regular rectilinear grids *Opt. Express* **20** 1247
- [22] Bohren C F *et al* 2008 *Absorption and Scattering of Light by Small Particles* (New York: Wiley)
- [23] Schafer J *et al* 2012 Calculation of the near fields for the scattering of electromagnetic waves by multiple infinite cylinders at perpendicular incidence *J. Quant. Spectrosc. Radiat. Transfer* **113** 2113
- [24] Palik E D 1998 *Handbook of Optical Constants of Solids* vol 3 (New York: Academic Press)
- [25] Johnson P B and Christy R-W 1972 Optical constants of the noble metals *Phys. Rev. B* **6** 4370
- [26] Bronstrup G *et al* 2010 Optical properties of individual silicon nanowires for photonic devices *ACS Nano* **4** 7113
- [27] Brönstrup G *et al* 2011 A precise optical determination of nanoscale diameters of semiconductor nanowires *Nanotechnology* **22** 385201
- [28] Li Y F *et al* 2015 Method to determine the optimal silicon nanowire length for photovoltaic devices *Appl. Phys. Lett.* **106** 091908
- [29] Traviss D J *et al* 2015 Antenna resonances in low aspect ratio semiconductor nanowires *Opt. Express* **23** 22771
- [30] Abujetas D R *et al* 2015 Unraveling the janus role of mie resonances and leaky/guided modes in semiconductor nanowire absorption for enhanced light harvesting *Accs Photonics* **2** 921
- [31] Anttu N and Xu H Q 2013 Efficient light management in vertical nanowire arrays for photovoltaics *Opt. Express* **21** A558
- [32] Chen Y *et al* 2016 Design for strong absorption in a nanowire array tandem solar cell *Sci. Rep.* **6** 32349
- [33] Sandhu S *et al* 2014 Detailed balance analysis and enhancement of open-circuit voltage in single-nanowire solar cells *Nano Lett.* **14** 1011
- [34] Cao L *et al* 2009 Engineering light absorption in semiconductor nanowire devices *Nat. Mater.* **8** 643
- [35] Cao L *et al* 2010 Tuning the color of silicon nanostructures *Nano Lett.* **10** 2649
- [36] Li Y *et al* 2016 Exact comprehensive equations for the photon management properties of silicon nanowire *Sci. Rep.* **6** 24847
- [37] Li Y *et al* 2016 Light harvesting of silicon nanostructure for solar cells application *Opt. Express* **24** A1075
- [38] Jain P K *et al* 2006 Calculated absorption and scattering properties of gold nanoparticles of different size, shape, and composition: applications in biological imaging and biomedicine *J. Phys. Chem. B* **110** 7238
- [39] Wang B and Leu P W 2012 Tunable and selective resonant absorption in vertical nanowires *Opt. Lett.* **37** 3756
- [40] Anttu N *et al* 2014 Crystal phase-dependent nanophotonic resonances in InAs nanowire arrays *Nano Lett.* **14** 5650
- [41] Metaferia W *et al* 2018 n-type doping and morphology of GaAs nanowires in Aerotaxy *Nanotechnology* **29** 285601